FAIMS Shotgun Lipidomics for Enhanced HILIC-like Separation and Automated Annotation of Gangliosides

Katharina Hohenwallner[1,2], Leonida M. Lamp[3], Liuyu Peng[4], Madison Nuske[4], Jürgen Hartler[3,5*], Gavin E. Reid[4,6,7*], Evelyn Rampler[1,2*]

1 Department of Analytical Chemistry, Faculty of Chemistry, University of Vienna, 1090 Vienna, Austria.

2 Vienna Doctoral School in Chemistry (DoSChem), University of Vienna, 1090 Vienna, Austria.

3 Institute of Pharmaceutical Sciences, University of Graz, 8010 Graz, Austria.

4 School of Chemistry, University of Melbourne, Parkville, Victoria 3010, Australia.

5 Field of Excellence BioHealth, University of Graz, 8010 Graz, Austria.

6 Department of Biochemistry and Pharmacology, University of Melbourne, Parkville, Victoria 3010, Australia.

7 Bio21 Molecular Science and Biotechnology Institute, University of Melbourne, Parkville, Victoria 3010, Australia.

ABSTRACT: The analysis of the glycosphingolipid subclass of gangliosides is extremely challenging, given their structural complexity, lack of reference standards, databases, and software solutions. Here, we introduce a fast 6 min High Field Asymmetric Ion Mobility Spectrometry (FAIMS) shotgun-based lipidomics workflow for improved ganglioside detection. By ramping compensation voltages, ideal ranges for different ganglioside classes were obtained. FAIMS revealed both class- and charge-state separation behavior based on the glycan head group moiety. The number of sialic acids attached to the glycan moiety correlated positively with their preferred charge state, i.e., trisialylated gangliosides (GT1-3) were mainly present as $[M-3H]^{3-}$ ions, whereas $[M-4H]^{4-}$ and $[M-5H]^{5-}$ ions were observed for GQ1 and GP1. $[M-5H]^{5-}$ ions were reported for the first time, primarily due to signal-to-noise enhancement and charge state filtering enabled by FAIMS. Overall, 11 ganglioside classes were covered i.e., GM1, GM2, GM3, GD1, GD2, GD3, GT1, GT2, GT3, GQ1, GP1. For data evaluation, we introduce a shotgun/FAIMS extension of the freely available, open-source Lipid Data Analyzer (LDA), which utilized combined orthogonal fragmentation spectra from CID, HCD, and 213 nm UVPD ion activation methods. Finally, 112 unique molecular gangliosides species were identified from pooled standards and porcine brain extracts. While conventional shotgun lipidomics favored the observation of singly charged ganglioside species, the incorporation of FAIMS yielded a higher number of annotated lipid species due to a gain in detection of multiply charged ion species. Therefore, this FAIMS-driven approach offers a promising strategy for complex ganglioside and glycosphingolipid characterization in shotgun lipidomics.

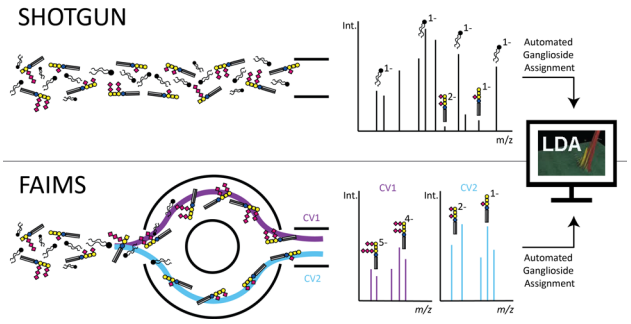

INTRODUCTION

Gangliosides, belonging to the acidic glycosphingolipids, are crucial players in cellular communication and neural function, predominantly present in the brain[1]. Located on the outer leaflet of the plasma membrane, these molecules contribute to neuronal development, cellular signaling, immune modulation, and show a significant impact on several diseases like cancer, Alzheimer's disease, and COVID-19[2,3]. Moreover, gangliosides have emerged as promising marker candidates in stem cell differentiation processes[4–7]. Structurally, gangliosides feature a lipid moiety (ceramide) and a highly variable glycan headgroup. Sialic acids, as part of the glycan moiety, impart negatively charged character at physiological pH values[8]. To date, ganglioside analysis remains highly challenging, given their enormous number of possible structures deriving from the combinations of the diverse and highly variable glycan and lipid moieties. This vast number of feasible structures are covered only to a limited extent by current software tools and databases, along with a limited availability of standards. In the realm of MS-based lipidomics, two predominant methodologies are employed for the analysis: shotgun lipidomics and liquid-chromatography mass spectrometry (LC-MS). Shotgun lipidomics offers the advantages of straightforward sample preparation, rapid analysis and high-throughput capabilities via the direct infusion of lipid extracts into the instrument[9]. One major limitation in ganglioside analysis, however, even when using ultra-high resolution mass spectrometry, is that signals of low abundance species cannot be distinguished in the presence of high abundance isomers and some isobars, due to the absence of orthogonal separation methods. This reduced specificity is especially pronounced when gangliosides and bulk lipids are analyzed simultaneously from the same sample matrix. Conversely, reversed-phase (RP) LC-MS introduces an additional dimension of separation for complex lipid mixtures[10]. The specific separation characteristics introduced by LC separation can be exploited by elution-based models such as the Equivalent Carbon Number (ECN) model[11–14] to distinguish between isobaric and isomeric species, enabling reliable identification of minor lipid species. A drawback of LC-MS lipidomics derives from longer analysis times, which can impede high sample throughput. Shotgun and LC-MS workflows tend to focus on specific ganglioside subsets, resulting in limitations for comprehensive profiling, or depend on long analysis times, and labor-intensive manual annotation[15–20]. However, due to the biological relevance of these analytes, there is an urgent need for comprehensive and fast deep-profiling approaches. The key for high-throughput and sensitive

MS-based glyco(sphingo)lipid and ganglioside analysis lies in reducing complexity, i.e., decreasing the number of species that result in a spectrum. This can be achieved by (1) faster LC-MS methods or (2) introducing an additional dimension of separation orthogonal to *m/z*, such as ion mobility spectrometry (IMS).

The general principle underlying IMS is the separation of ions based on their mobility in an electric field, which depends on their size, shape, and charge. The electric field can either be (1) static or (2) oscillating. Furthermore, there are two main separation techniques applied: (1) temporal and (2) spatial separation. The temporal separation gathers information about all ions present at the time of the scan providing information on the arrival time for each ion. The spatial separation acts as a filter, allowing only ions with specific characteristics to pass. By consecutive scanning with different settings a comprehensive view of the ions present can be obtained, as each setting selectively allows specific ions to pass. Several devices with different combinations of the applied electric field and separation technique are commercially available[21,22].

Numerous studies using IMS based on temporal-separation have been reported for the analysis of gangliosides, offering separation of isomeric ganglioside species and deep characterization of the ganglioside lipidome [16,17,23–34]. In contrast, spatial-separation based IMS for gangliosides analysis has received limited attention [35], despite its potential for increased sensitivity as shown in proteomics and lipidomics studies[36–44]. Overall, ganglioside analysis approaches aim for high-confidence identifications, requiring accurate mass, MS/MS fragment information, and, ideally, matching database entries or a reference standard[45]. Collision-Induced Dissociation (CID) and High-energy Collisional Dissociation (HCD) are the most commonly used ion activation methods for MS/MS lipid structural analysis. However, Ultraviolet Photodissociation (UVPD)-MS^n represents a cutting-edge technique that provides almost complete structural characterization across multiple lipid categories and classes, including localizing double bond positions, cyclization and other acyl chain modifications, and assignment of *sn*-linkage positions[39,46–57].

A major bottleneck of ganglioside and glyco(sphingo)lipid data analysis is molecular assignment and correct annotation using accurate mass and MS/MS information, which often relies on tedious manual annotation of fragmentation spectra. In 2022, a seminal review provided a comprehensive overview of freely available tools for lipidomics MS-based data analysis[58], including tools dedicated for the analysis of shotgun data[59]. Data evaluation tools for ganglioside based on FAIMS shotgun lipidomics are currently inapplicable for our purpose, because (1) databases entries are limited, (2) higher charge states are completely absent, (3) the available sphingolipid species are exclusively dihydroxylated. Additionally, most tools focus either on shotgun or LC data evaluation and are not explicitly designed for FAIMS. Recently, we demonstrated automated annotation of fragmentation spectra for gangliosides using LC-MS and decision rules[7]. Here we introduce a newly developed shotgun/FAIMS extension of the freely available software LDA[60–62]. Importantly, the presented software and the developed decision rules can be applied to both conventional shotgun and FAIMS-based data[7], while also supporting UVPD and other orthogonal fragmentation techniques. In this study, we demonstrate the capability of shotgun mass spectrometry (MS) coupled with spatial-separation-based FAIMS for the enhanced identification of gangliosides. Our investigation further encompasses CID, HCD, and UVPD as fragmentation techniques. We explore the structural insights provided by each fragmentation method and specifically compare the spectral quality between results obtained using shotgun MS approaches, with and without FAIMS. Moreover, we present for the first time an automated solution for annotating ganglioside UVPD data acquired by our FAIMS shotgun approach, which fully exploits the significantly increased sensitivity and flexibility of our method.

EXPERIMENTAL SECTION

Standards and Solvents. All solvents were of LC–MS grade. HPLC grade chloroform ($CHCl_3$) was purchased from Ajax Finechem. Butylated hydroxytoluene (BHT), isopropanol (IPA), MS grade methanol (MeOH) and acetonitrile (ACN) were purchased from Merck. Ganglioside standards were obtained from Cayman Chemical, Avanti Polar Lipids, and Merck. A pooled ganglioside standard (PGS) including 12 standards with a final concentration of approximately 5 µM was prepared in either (1) 4:2:1 IPA/MeOH/$CHCL_3$ (v/v/v) with 20 mM ammonium formate (AF, ChemSupply) or (2) pure 4:2:1 IPA/MeOH/ $CHCL_3$ (v/v/v), without the addition of AF. Additionally, a total porcine brain extract (BE, Avanti) was chosen as complex proof-of-concept sample. The BE sample was diluted to a final concentration of 250 µg/mL in the two IPA solvent mixtures described above. All standards used in this study are listed in Supplementary Table 1.

Mass spectrometry. In this study, the value of FAIMS for ganglioside analysis has been evaluated in relation to conventional shotgun (referred to as noFAIMS) analysis. Instrument parameters for both setups were optimized, with a focus on spray current, ion transfer tube temperature and the applied RF voltage (Supplementary Figure 1). For shotgun analysis, nano electrospray ionization (nESI) using a TriVersa NanoMate (Advion BioSciences, Ithaca, NY, USA) was coupled to an Orbitrap Fusion Lumos mass spectrometer (Thermo Fisher, San Jose, CA, USA). The mass spectrometer (MS) was expanded with a user-installed 213 nm laser (Ekspla NL204, 0.2 mJ, 7-10 ns pulse duration, 1 kHz repetition rate, Vilnius, Lithuania) for UVPD fragmentation. For Full Scan (MS1) experiments, the system was operated in negative ionization mode with a spray voltage of 1.3 kV, and a gas pressure of 0.3 psi. The heated transfer capillary was set to a temperature of 170 °C, the radio frequency (RF) voltage was adjusted to 60% and the scan range was set to *m/z* 250-2,000 using quadrupole isolation and an Orbitrap mass resolving power of 120,000 (at *m/z* 200). The Automatic Gain Control (AGC) target was set to standard, and the maximum injection time (MIT) was limited to 100 ms. The scan number was consistently set to 50. Additionally, we developed a 3.5-minute automated data-dependent acquisition (DDA) MS/MS method, which includes CID, HCD and UVPD fragmentation for a ganglioside-specific inclusion list (see Supplementary Figure 2). In detail, 30 seconds MS1 acquisition was followed by 60 seconds DDA CID (27%, 10 ms, Q=25), DDA HCD (27%) and DDA UVPD (17 ms) each. These DDA scans were executed in an unscheduled mode using the ganglioside-specific inclusion list with a mass tolerance of 5 ppm and a dynamic exclusion of 10 seconds. The cycle time was set to 8 seconds, and an intensity threshold of 8.0e3 for the precursor was applied. The Orbitrap mass resolving power was set to 60,000, the *m/z* range to 150-2,000, with an isolation window of 1.5, 1 microscan, an AGC target of 100% and 300 ms MIT.

For FAIMS measurements, a FAIMS Pro source (Thermo Scientific, Waltham, MA, USA) was used. The spray voltage was set to 1.6 kV, all other parameters were kept constant (see shotgun method above). For MS1, a 2.7 min compensation voltage (CV) scan was designed, starting at a CV of 25 V and reaching 77 V. Each specific CV value was maintained for 6 seconds before an incremental increase of 2 V in each step. Additionally, a 6-minute DDA experiment was conducted for ganglioside identification. Optimized for GD1 gangliosides, the FAIMS CV was fixed at 45 V for 30 seconds for MS1 scans, followed by CID, HCD and UVDP for 30 seconds each, with the same settings as described for the noFAIMS setup. From minute 2 to 6, DDA UVPD experiments were performed at different CVs with incremental steps from 35 V to 67 V, with each voltage (35 V, 39 V, 45 V, 55 V, 59 V, 63 V, 67 V) held for 30 seconds.

The PGS and BE samples were measured in triplicate, with both solvent mixtures (i.e., AF and noAF) and both instrument setups (i.e., FAIMS and noFAIMS), along with solvent blanks and QC samples. In-depth explanation of the methodology, along with visual representations and screenshots from the method editing software, can be accessed in the Extended Methods section in the Supplementary Materials (Supplementary Table 2-4 and Supplementary Figure 2-7).

Development of a new LDA shotgun/FAIMS extension. As part of this work, LDA[62], which was originally designed for the analysis of chromatography-based MS data, has been extended for the analysis of conventional shotgun and shotgun FAIMS data. This extension comprises an MS1 shotgun quantitation module and a module for isotope correction. For shotgun data, the MS1 quantitation module substitutes LDA's conventional MS1 quantitation (based on 3D peak deconvolution[60]) by a shotgun specific quantitation based on MS1 intensities. This module extracts for each analyte/ion species combination (*m/z* values provided in an extensible Excel mass list) the measured intensities that fall within a user-settable tolerance around the monoisotopic *m/z* value of interest (m+0) plus a definable number of isotopologues (m+1, m+2, etc.). For calculating a quantitative surrogate for each isotopologue out of these intensities, three methods are provided, i.e., the 'median', the 'mean', and the 'sum'. Subsequently, LDA's isotope correction routine can be applied. The isotope correction routine works in an iterative manner. It starts with species unaffected by the isotopes of other species, calculates the theoretical values of each isotope (based on the theoretical isotope intensity distribution) of up to m+5, and corrects all the isotopes of other species that show an overlap to the *m/z* values of any of these isotopes (from the unaffected species). These theoretical isotope intensities are calculated in relation to the monoisotopic m+0 intensity. The m+0 can be either the measured m+0 intensity, or, if the m+1 has been quantified also, it is the mean of the measured m+0 intensity and a hypothetical m+0 intensity calculated from the measured m+1 intensity. This second calculus may be useful to reduce errors introduced by isotopes of other species, because the m+1 intensity is typically less affected by isotopic overlaps than the monoisotopic m+0 intensity. Then, the algorithm iteratively continues the same procedure with species which reached the 'unaffected by other isotopes' status post correction until there are no more species left for correction. Notably, LDA differentiates between species 'unaffected' and 'affected' by isotopologues originating from other species, and it does not simply start out at species with the lowest *m/z* value. This is particularly important for e.g., fully ^{13}C labeled species, which tend to show isotopic distributions in negative *m/z* direction due to ^{12}C impurities. Subsequent to MS1 quantitation, the MS2 information is evaluated based on decision rule sets[61]. In a final step, the quantities assessed for the lipid species (sum composition level post isotope correction) are split among the individual lipid molecular species (fatty acid isomers) based on the distinct fragments of each species (for details see 'Application 3' of Online Methods of the LDA2 publication[61]).

Automated data evaluation using LDA. Full MS scans of PGS and BE under all 4 study setups (AF_noFAIMS, noAF_noFAIMS, AF_FAIMS, and noAF_noFAIMS) were evaluated in Skyline (MacCoss Lab, version 23.1.0.268)[63] to generate a ganglioside suspect list for further analysis. Dihydroxylated species with ceramide lengths from 30 to 46 carbons with 0 to 2 double bonds from 11 ganglioside classes (GM1, GM2, GM3, GD1, GD2, GD3, GT1, GT2, GT3, GQ1, and GP1) were considered. This pre-selection is based on experience obtained from previous LC-MS measurements. Only species present in all three replicates in at least one sample group (PGS or BE) under one study condition (i.e., AF_noFAIMS, noAF_noFAIMS, AF_FAIMS, and noAF_noFAIMS) and with a minimum of 10 datapoints were considered for the generation of the suspect list.

To confirm the validity of the suspects, Full MS and DDA scans were analyzed using LDA's shotgun/FAIMS extension described above (version 2.10). The ganglioside specific mass list[7] was limited to the suspects, and the following ion species were searched for: $[M-H]^-$, $[M-2H+Na]^-$, $[M-2H]^{2-}$, $[M-3H]^{3-}$ and $[M-4H]^{4-}$. We applied an *m/z* tolerance of 5 ppm and 0.2 Da for the analysis of MS1 and MS/MS data, respectively (these settings are activated in LDA version 2.10 by selecting the instrument 'OrbiTrap_Lumos_shotgun' and the fragmentation selection 'Ganglioside_neg_shotgunFAIMS'). For MS1 quantitation, we obtained the isotope corrected intensities (m+0 and m+1 isotopologues) using the 'sum' mode. The evaluation was performed on CID, HCD and UVPD spectra, as well as combined spectra comprising all three ion activation methods, since the combination proved to be most informative for our purpose. Ganglioside species annotation and quantitation were performed automatedly by LDA. Only species verified by MS2 annotations were used for further data processing. Using the rdb export option available in the LDA software, the data was further processed and visualized using R Studio (version 4.3.2) and Illustrator (Adobe Inc., version 28.2, 2023). For R Studio code optimization and refinement, ChatGPT (GPT-3.5, OpenAI, 2023) was used. FreeStyle (Thermo Fisher, 1.8 SP2 QF1, version 1.8.65.0) was used for quality control and visualization along the whole data evaluation process

RESULTS AND DISCUSSION

The structural complexity of gangliosides and glycosphingolipids complicates their analysis using shotgun high-resolution mass spectrometry-based workflows. By introducing FAIMS separation prior to shotgun analysis, MS spectra complexity is reduced, enabling fast and sensitive ganglioside analysis. Applying FAIMS with combined fragmentation techniques (UVPD, HCD, CID) enabled enhanced HILIC-like separation and automated ganglioside annotation.

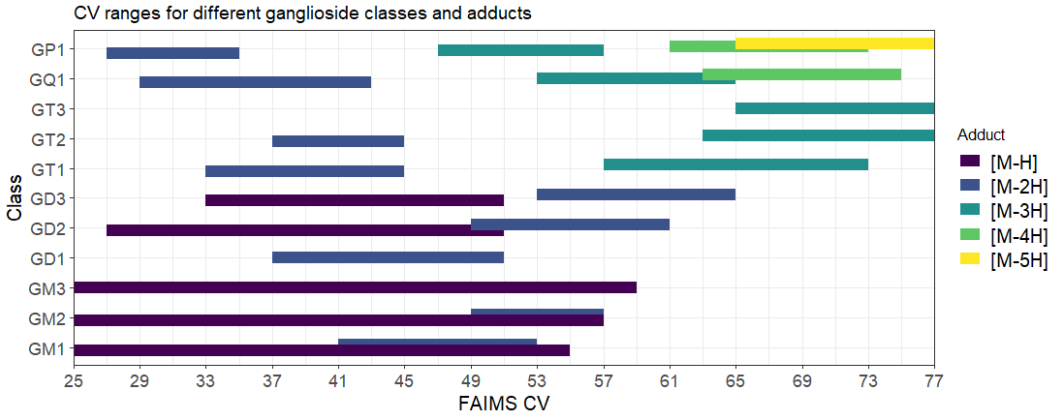

Figure 1. Visualization of CV ranges for each ganglioside class and their corresponding ion species measured in negative ion mode by FAIMS shotgun lipidomics with and without ammonium formate (AF). All ganglioside classes can form multiple ion species with different charge states (ranging from $[M-H]^-$ to $[M-5H]^{5-}$, depending on the specific class). The predominant ion species correlates with the number of sialic acids: GM1-3 species favor the formation of $[M-H]^-$, while GD1-3 species favor $[M-2H]^{2-}$, GT1-3 $[M-3H]^{3-}$, GQ1 $[M-4H]^{4-}$, and GP1 $[M-5H]^{5-}$. Generally, lower CV values promote ions at lower charge states, while higher CV values display multiply-charged species. A dependency of ion formation on the presence or absence of AF was observed. The addition of AF promoted the detection of lower-charge state ions, e.g. $[M-2H]^{2-}$ for GQ1 and GP1 was only observed with AF containing solvent. As expected, the absence of AF resulted in the detection of higher-charge state ions, e.g., $[M-4H]^{4-}$ and $[M-5H]^{5-}$ for GQ1 or GP1 were only observed at solvents lacking AF.

FAIMS FOR ENHANCED SHOTGUN GANGLIOSIDE DETECTION. To implement shotgun FAIMS for ganglioside detection, fine-tuning of parameters such as sample introduction conditions, ion optics, and spray voltages was essential. Our method optimization demonstrated a substantial enhancement in signal-response by increasing the RF voltage (Supplementary Figure 1). As no additional in-source fragment formation occurred, general stability of gangliosides within the optimized method was assumed.

Evaluation of FAIMS CV ranges for different ganglioside classes and charge states. In this study, we explored the compensation voltage (CV) parameter in FAIMS as an additional separation dimension for shotgun lipidomics analysis. 11 ganglioside classes, which comprise GM1, GM2, GM3, GD1, GD2, GD3, GT1, GT2, GT3, GQ1, and GP1, were covered. A FAIMS CV screening method ranging from 25 to 77 V showed that each ganglioside class generally possesses an optimal CV range rather than a narrowly confined voltage requirement. For example, for GD1 $[M-2H]^{2-}$, a CV range from 37-51 V and for GT1 $[M-3H]^{3-}$, CV ranges from 57-73 V were found to be optimal. Notably, singly charged species were obtained in broader CV ranges as illustrated for GM1, GM2, and GM3 in Figure 1. Additionally, correlation was observed between the number of sialic acids and the most abundant charge state. Singly charged species were dominated by GM1, GM2 and GM3 (single sialic acid) gangliosides, while GD1, GD2 and GD3 (two sialic acids) were observed primarily as doubly charged species. Following this trend, triply charged species were detected for GT1, GT2 and GT3 (three sialic acids), quadruply charged species for GQ1 (four sialic acids) and even quintuply charged species for GP1 (five sialic acids). While quadruply charged ion species for several GQ1 species have been described[17], quintuply charged species have not previously been reported for gangliosides. A table with the specific CV ranges for each ganglioside class and their respective charge states can be found in Supplementary Table 5. Another interesting observation was that the presence or absence of ammonium formate (AF) in the solvent mixture influenced the ion species formation. We observed that AF containing samples favored the formation of lower charged species, while higher charged ions were predominantly detected in the absence of AF.

FAIMS provides class and charge separation. Applying the FAIMS source enabled class-specific separation of gangliosides based on the glycan head group (Figure 2a). Two primary factors affect the CV range for a ganglioside class: (1) the total sugar length and (2) the number of sialic acids. Notably, a reduction in total sugar length from GD1 to GD2 to GD3 corresponded to an increase in the optimal FAIMS CV (Figure 1 and Figure 2a). Conversely, as illustrated with GT1, GD1, and GM1, an increase in sialic acid content correlated with a lower FAIMS CV range, highlighting the significance of glycan composition in separation dynamics. Notably, all species within a class exhibited the same CV range (Figure 2b) i.e., the total ceramide length and number of double bonds did not influence the CV range for their transmission, as demonstrated with various GD1 lipid species. The head group separation observed in FAIMS coupled with the absence of ceramide-based separation offers similar benefits as Hydrophilic Interaction Liquid Chromatography (HILIC) in LC-MS. Correspondingly, FAIMS can be seen as a 'HILIC-like' separation modality for shotgun lipidomics with an additional layer of specificity to enhance the characterization of complex (glycosphingo)lipid mixtures. In addition, FAIMS also enables separation of species based on charge-state. Varying CV ranges for distinct charge states are exhibited, with higher charge states requiring higher CV ranges (Figure 2c). As illustrated by the example of 38:1;O2 for the classes GP1, GQ1, and GT1, differently charged ion species are detectable at different CV ranges, following the above-mentioned direct correlation. Notably, the CV range for a specific class and ion species provided excellent. reproducibility, as the values exhibited stability within a sequence and remained consistent in inter-day comparisons. This reproducibility aligns with the principles of FAIMS, where the CV is a critical parameter utilized for spatial separation based on variations in electric fields. In summary, spatial-separation based FAIMS, in the context of ganglioside analysis, is primarily influenced by the glycan head group (total sugar length and sialic acid quantity) and charge state, resulting in HILIC-like class separation with an additional dimension for charge state separation.

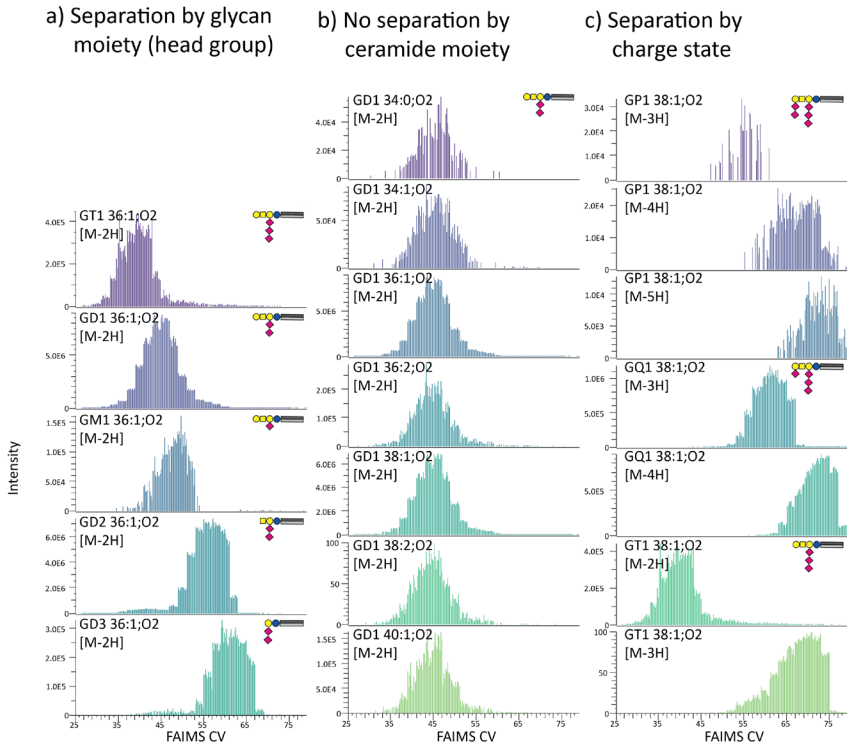

Figure 2. Effect of FAIMS CV range based on the (a) glycan head group, (b) ceramide moiety and the (c) charge state. Similar to HILIC separations in LC-MS, FAIMS provides separation based on the (a) head group, but (b) not on the ceramide moiety. A higher total sugar length correlates with lower CV ranges, while lower sialic acid numbers lead to higher CV ranges. An additional separation dimension is introduced by the charge state (c), with a direct correlation of lower CVs for lower charge states and higher CVs for higher charge states. The presented data is acquired from the pooled ganglioside standard analyzed in MS1 without AF in the solvent.

FAIMS improves signal-to-noise and enhances the spectral quality. The impact of FAIMS on both MS1 (signal-to-noise ratio (S/N)) and MS/MS (spectral quality) was examined using a complex porcine brain extract (BE). While the conventional shotgun (noFAIMS) approach enabled observation of the complete brain lipidome, FAIMS enabled the specific extraction of certain classes and charge states depending on the selected CV (see Figure 1 and 2, as well as Supplementary Figure 8 and 10). For example, when higher CVs were applied, FAIMS drastically reduced the sample complexity by excluding all singly charged bulk lipids (compare Figures 3b and 3a). This leads to a significant S/N improvement for ganglioside analysis by FAIMS. FAIMS enabled the detection of highly charged ganglioside species e.g., several GQs and GTs (Figure 3b) which were not detected by conventional shotgun lipidomics analysis (Figure 3a). As previously reported for peptides[64,65], FAIMS demonstrates its applicability for enhanced identification, particularly for enriching highly charged species. The reduction of spectral complexity and the sensitivity enhancement induced by the electric field-based FAIMS separation is especially valuable in complex samples, as isomeric and isobaric overlap amongst lower charged species can be eliminated. This finding is additionally illustrated in Supplementary Figures 8-10 for GQ1 38:1;O2 and GD1 36:1;O2, where the application of FAIMS resulted in a clean isotopic fine structure for GQ1 38:1;O2 (no overlaps compared to the conventional shotgun approach), and transforms a hybrid MS/MS spectrum into a clean spectrum for GD1 36:1;O2. As the value of a method cannot be fully evaluated by a small set of analytes, we aimed to annotate a broad range of different ganglioside classes and species. To date, the assignment of annotations (MS1 and MS/MS) for gangliosides, and glycolipids in general, is predominantly performed manually, especially in shotgun experiments. We previously introduced an LC-MS-based, automated annotation pipeline for gangliosides utilizing LDA[7]. In the present study, we extended LDA for annotating the obtained shotgun and FAIMS data to perform annotation of a broad range of ganglioside species in a complex mixture using various ion activation techniques.

ENHANCING AUTOMATED GANGLIOSIDE ANNOTATION. A lack of standards, fragment databases, and automated software solutions demands tedious spectra annotation processes, which have to be performed manually to a large extent. To overcome these challenges, we introduce an automated workflow for ganglioside annotation using the newly developed LDA extension, capable of analyzing MS and MS/MS shotgun and FAIMS data.

LDA for automated shotgun FAIMS ganglioside annotation. Whenever a study requires the exploitation of previously undetected ion species, such as the higher negatively charged gangliosides presented in this study, or novel fragmentation techniques like UVPD, automated annotation by conventional software is usually not supported. This is primarily attributed to the absence of informative ions within the databases utilized by these tools. This situation becomes even more challenging when orthogonal separation methods such as FAIMS are used, which are beyond mainstream data analysis. Under these circumstances, flexible and easily expandable solutions become particularly important. The LDA offers a highly adaptable solution by using decision rules[61]. Moreover, since target mass lists of lists can be easily extended to any conceivable lipid class and ion species. Besides, LDA supports annotations at the lipid

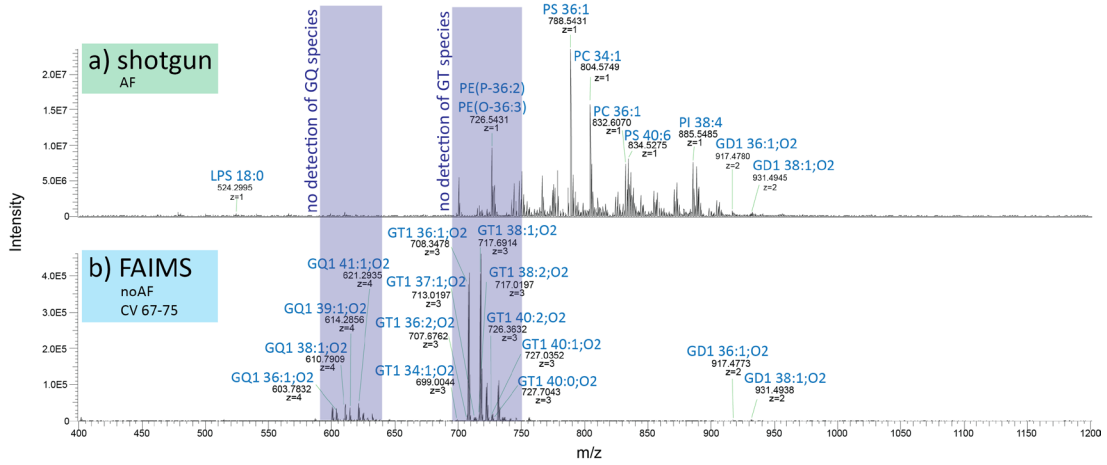

Figure 3. Comparison of ganglioside detection (MS1) in the porcine brain extract (BE) with (a) the conventional shotgun lipidomics workflow using AF as modifier and (b) the FAIMS-based approach without AF. Singly charged bulk lipids can be detected by the conventional shotgun method, but ganglioside species can be hardly observed, particularly species preferring higher charge states. Conversely, FAIMS enables access to the multiply charged ganglioside species. Improvement of the S/N by FAIMS is evident by the detection of the multiply charged GQ and GT species, which were not detected with the conventional shotgun approach.

molecular species level, as well as additional hydroxylation states apart from dihydroxylated species[62], provides visualization, and extensive export options (Excel, tab delimited text, rdb, mzTab-M[66], image formats). To exploit these advantages for shotgun and FAIMS/shotgun data, we developed LDA's shotgun/FAIMS extension (see Materials and Methods) and tested its usability on pooled ganglioside standards and a porcine brain extract.

Increased structural information by combining CID, HCD, and UVPD fragmentation spectra. In both shotgun and shotgun FAIMS workflows, we explored CID-, HCD-, and UVPD-MS/MS as distinct fragmentation techniques. This strategy facilitated (1) the comparison of different fragmentation techniques and (2) an increase in the structural information gain by combining MS/MS spectra in an averaged (LDA, Freestyle) or sum (LDA) spectrum, exemplified in Figure 4c by the example of GD1 36:1;O2. While most fragments could be obtained with all three fragmentation techniques, UVPD resulted in an overall increase in the number of observed fragments. Particularly glycan-specific head group fragments were predominantly observed using UVPD (Figure 4b). Nonetheless, the three possible glycan isomers of GD1 remain indistinguishable by shotgun lipidomics (Figure 4a), due to missing separation. However, isomers on the ceramide moiety can be elucidated, as demonstrated in Figure 4c. Molecular lipid species identification, primarily achieved through UVPD, but also occasionally with HCD and CID (FA/SPB detection), was possible for several highly abundant gangliosides. However, certain fragments, such as the G- fragment[46] (neutral loss of FA from precursor), were exclusively obtained via UVPD. Each fragmentation technique generated ganglioside-specific diagnostic fragments, such as *m/z* 290.0876, representing sialic acid (NeuAc). Despite expectations based on previously detected double-bond positions in sulfatides and glycerophospholipids[46,47], we could not detect double-bond positions or cross-ring (A, X) fragments with UVPD. Their absence may be attributed to the low abundance of ganglioside species in the sample[47]. In total, 112 unique ganglioside species could be annotated in the standard pool, applying the LDA shotgun extension to both instrument setups and both solvent mixtures (see Table 1 and Supplementary Table 6). In detail, 56 ganglioside species of the classes GD1-3, GT1-3, GQ1 and GP1 could be annotated with shotgun (noFAIMS), and 87 with FAIMS. As mentioned above, the presence or absence of ammonium formate (AF) in the solvent mixture influenced the ion species formation. While the stability of the nESI spray remained unaffected by this modification, the absence of AF seemingly enhanced the spray stability in FAIMS injections. Furthermore, since the observed charge states depend on AF and the instrument setup, these factors influenced the number of identifications. Ganglioside classes predominantly present as singly charged ions (GM1, GM2, GM3) were promoted by adding AF. The traditional shotgun approach with AF yielded 25 annotated monosialylated ganglioside species, while the application of FAIMS reduced the number to 16 and 19, with and without AF, respectively. Overall, 6 ganglioside species, belonging to monosialyated gangliosides were only detectable when the conventional shotgun lipidomics workflow was used. In contrast, the novel FAIMS approach uniquely identified 31 species from classes that promote the formation of higher charged ion species, particularly in the absence of AF. This result confirms the advantage of adding AF for conventional lipidomics shotgun analysis[67], focusing on singly charged bulk lipids. At the same time, it provides an explanation as to why most shotgun and LC-MS non-targeted lipidomics workflows primarily detect GM3 or other monosialylated ganglioside classes, while being not capable of detecting higher sialylated ganglioside classes[68–71]. This underlines the importance of sample preparation and method optimization and leads to the conclusion that salt addition in solvent mixtures should be optimized for the analytes of interest, prior to analysis.

Proof-of-principle: ganglioside profiling of porcine brain. The utility of FAIMS is particularly evident in the analysis of higher negatively charged gangliosides. The porcine brain extract serves as a complex biological matrix, predominantly consisting of singly charged bulk lipids (as illustrated in Figure 3a). In the presence of so many 'noise' lipids, we demonstrate the capabilities of FAIMS in enhancing the detection of gangliosides, as the increased sensitivity and improved spectral quality described above also contribute to higher numbers of ganglioside identifications for the complex porcine brain (BE) extract. 44 unique ganglioside species of 7 different classes, namely GM1, GD1, GD2, GD3, GT1, GT3, and GQ1 could be annotated (see Table 1). With the shotgun setups, slightly less (25) species were detected with AF, compared to the absence of

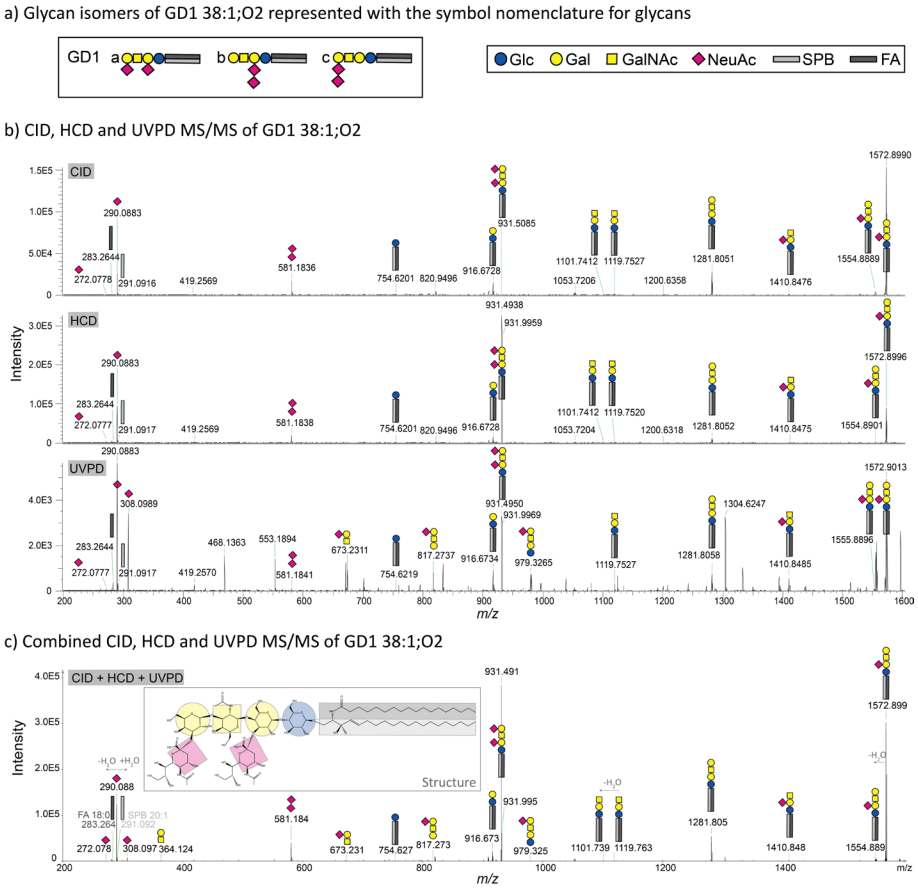

Figure 4. (a) Glycan isomers of GD1 and symbol legend. Glc=glucose, Gal=galactose, GalNAc=N-acetylgalactosamine, NeuAc=Neuraminic Acid/sialic acid, SPB= sphingoid base[72], FA=fatty acid. MS/MS (average of 50 scans) for GD1 36:1;O2 in the porcine brain sample using (b) CID, HCD, or UVPD as fragmentation technique. (c) Combined MS/MS spectrum consisting accumulated (sum) of spectra acquired by all three fragmentation techniques. All assignments were automatically done by the newly developed LDA extension using shotgun FAIMS data without the addition of AF. For visualization, the annotations are represented with the glycan symbol nomenclature [73,74].

AF (29). The same trend occurred in the FAIMS setup with 39 and 44 annotations with and without AF, respectively. Overall, FAIMS without AF was superior to the other methods, which is particularly prominent for GQ1 and GT3 species, which were exclusively detected by FAIMS without AF. FAIMS provides increased coverage of gangliosides as it facilitates the detection of low abundance, higher charge state ganglioside classes. Our findings are in accordance with literature as GM1, GD1, GD2, GD3 and GT1 have been reported in several studies as the main ganglioside classes present in the human brain[2,75]. GT3 and GQ1 are less commonly discussed, however, both classes have been described in human brain[17], and early ganglioside studies already described GT3 in fish brain[76], and GQ1 in rat brain[77]. The increased number of identifications with FAIMS in a complex biological sample dominated by singly charged molecules highlights the enhancement in sensitivity towards analytes occurring at higher charge states. The advantages of FAIMS in complex samples is further exemplified in the extended methods section, demonstrated with GQ1 38:1;O2. The annotation of this analyte via MS/MS was exclusively achievable using FAIMS emphasizing the general efficacy of FAIMS for the detection and annotation of gangliosides. For a comprehensive list of all detected ganglioside species, including method setup details and information on detected ion species in both BE and PGS refer to Supplementary Table 6.

In summary, the application of FAIMS in shotgun analysis enabled fast and comprehensive ganglioside profiling. We could demonstrate HILIC-like characteristics (separation based on the head group) and additionally charge state separations for the FAIMS setup. This ultimately led to an increase in sensitivity and improvement in spectral quality, which resulted in higher number of annotations in pooled standards and complex brain extracts by using FAIMS, complemented by the presented automated LDA solution.

CONCLUSION

FAIMS shotgun lipidomics offers rapid class- and charge-based separation of gangliosides providing increased S/N ratios and unprecedented clear signals of multiply charged ganglioside species in the presence of abundant bulk lipids. The class-specific ganglioside separation and charge state trends exploitable by FAIMS, and the MS/MS-based structural information provided by CID, HCD, and UVPD enhanced the annotation of ganglioside lipids in pooled standards and porcine brain samples. While shotgun lipidomics in the absence of FAIMS favored singly charged gangliosides and bulk lipids, the application of FAIMS led to the enhanced detection of multiply charged species for ganglioside classes with higher sialylation state. In summary, this study provided for the first time a clear strategy to reproducibly exploit FAIMS compensation voltages

Table 1. Total numbers of annotation for the pooled ganglioside standard (PGS) and the brain extract (BE)[a].

Sample	GM1	GM2	GM3	GD1	GD2	GD3	GT1	GT2	GT3	GQ1	GP1	IDs	Total
PGS/AF/noFAIMS	4	2	19	7	11	20	5	2	0	0	0	70	112
PGS/noAF/FAIMS	2	1	16	7	11	26	5	2	0	3	2	75	
PGS/AF/FAIMS	4	2	12	13	15	30	12	4	0	5	2	99	
PGS/noAF/FAIMS	4	2	13	13	15	30	12	4	5	6	2	106	
BE/AF/noFAIMS	2	0	0	7	2	9	5	0	0	0	0	25	44
BE/noAF/FAIMS	2	0	0	7	2	10	5	0	0	3	0	29	
BE/AF/FAIMS	2	0	0	11	2	10	11	0	0	3	0	39	
BE/noAF/FAIMS	2	0	0	11	2	10	11	0	4	4	0	44	
Ion Species	$[M-H]^-$	$[M-H]^-$	$[M-H]^-$	$[M-2H]^{2-}$	$[M-2H]^{2-}$	$[M-2H]^{2-}$	$[M-3H]^{3-}$	$[M-2H]^{2-}$ $[M-3H]^{3-}$	$[M-3H]^{3-}$	$[M-3H]^{3-}$ $[M-4H]^{4-}$	$[M-4H]^{4-}$ $[M-5H]^{5-}$		

[a]The numbers are demonstrated for different ganglioside classes along with the main ion species detected.

for unambiguous class and charge state separation of gangliosides. The introduced concept of CV range class-based separation for medium to high mass range (glycosphingo)lipids can be applied as quality check filter criteria similar to the ECN model. Moreover, the presented FAIMS shotgun workflow is completed by a software solution for fully automated annotation. As such, we anticipate that our work can be easily utilized by anybody interested in in-depth analysis of gangliosides. Overall, FAIMS shotgun lipidomics, particularly when coupled with advanced MS/MS methods, is a promising tool for the enhanced separation and structural annotation of multiply charged molecules and it is particularly beneficial for glycolipids.

ASSOCIATED CONTENT

Supporting Information

Extended experimental section and supporting tables and figures (Supporting_Info.pdf). Installation and download instructions for LDA 2.10, as well as access to study data, will be available upon publication.

AUTHOR INFORMATION

Corresponding Author

*Evelyn Rampler – evelyn.rampler@univie.ac.at
*Gavin E. Reid – gavin.reid@unimelb.edu.au
*Jürgen Hartler – juergen.hartler@uni-graz.at

Author Contributions

The methodology was implemented by K.H., M.N., and L.P. The formal analysis, including sample preparation, data acquisition and data evaluation, were performed by K.H. Figures and tables for data visualization were prepared by K.H. and supported by E.R., and G.E.R. Analytical instrumentation, lab resources and student supervision were provided by J.H., G.E.R and E.R. The LDA extension was developed by K.H., L.M.L., and J.H. Funding acquisition, conceptualization, and project management were performed by K.H. (DosChem grant), E.R. and G.E.R. The original draft writing was performed by K.H. and E.R followed by manuscript revision and editing by all authors All authors have given approval to the final version of the manuscript.

Notes

The authors declare no competing financial interest.

ACKNOWLEDGMENT

K.H. was financed by the Austrian Science Fonds (FWF) within the research group program (grant FG3) and a travel grant of the Doctoral School of Chemistry (DosChem) of the University of Vienna, Faculty of Chemistry. The research was funded in part by the Australian Research Council, grant number DP190102464 to G.E.R. The authors thank all members of the Reid lab (University of Melbourne), Rampler lab and Koellensperger lab (University of Vienna) as well as the Hartler lab (University of Graz) for the great team spirit and scientific exchange across continents. We also thank Dr Shuai Nie and Huaqi Su for their scientific exchange and support with respect to the instrumentation located within the Mass Spectrometry and Proteomics Facility (MSPF) at the Bio21 Institute, University of Melbourne, where the study was performed.

REFERENCES

(1) Schnaar, R. L. Glycolipid-Mediated Cell–Cell Recognition in Inflammation and Nerve Regeneration. *Arch Biochem Biophys* **2004**, *426* (2), 163–172. https://doi.org/10.1016/J.ABB.2004.02.019.

(2) Sipione, S.; Monyror, J.; Galleguillos, D.; Steinberg, N.; Kadam, V. Gangliosides in the Brain: Physiology, Pathophysiology and Therapeutic Applications. *Front Neurosci* **2020**, *14*. https://doi.org/10.3389/FNINS.2020.572965.

(3) McQuaid, C.; Solorzano, A.; Dickerson, I.; Deane, R. Uptake of Severe Acute Respiratory Syndrome Coronavirus 2 Spike Protein Mediated by Angiotensin Converting Enzyme 2 and Ganglioside in Human Cerebrovascular Cells. *Front Neurosci* **2023**, *17*, 1117845. https://doi.org/10.3389/FNINS.2023.1117845/FULL.

(4) Liang, Y. J.; Kuo, H. H.; Lin, C. H.; Chen, Y. Y.; Yang, B. C.; Cheng, Y. Y.; Yu, A. L.; Khoo, K. H.; Yu, J. Switching of the Core Structures of Glycosphingolipids from Globo- and Lacto- to Ganglio-Series upon Human Embryonic Stem Cell Differentiation. *Proc Natl Acad Sci U S A* **2010**, *107* (52), 22564–22569. https://doi.org/10.1073/PNAS.1007290108/SUPPL_FILE/PNAS.201007290SI.PDF.

(5) Bergante, S.; Torretta, E.; Creo, P.; Sessarego, N.; Papini, N.; Piccoli, M.; Fania, C.; Cirillo, F.; Conforti, E.; Ghiroldi, A.; Tringali, C.; Venerando, B.; Ibatici, A.; Gelfi, C.; Tettamanti, G.; Anastasia, L. Gangliosides as a Potential New Class of Stem Cell Markers: The Case of GD1a in Human Bone Marrow Mesenchymal Stem Cells. *J Lipid Res* **2014**, *55* (3), 549. https://doi.org/10.1194/JLR.M046672.

(6) Park, J.; Lee, Y.; Shin, J.; Lee, H. J.; Son, Y. B.; Park, B. W.; Kim, D.; Rho, G. J.; Kang, E. Mitochondrial Genome Mutations in Mesenchymal Stem Cells Derived from Human Dental Induced Pluripotent Stem Cells. *BMB Rep* **2019**, *52* (12), 689. https://doi.org/10.5483/BMBREP.2019.52.12.045.

(7) Hohenwallner, K.; Troppmair, N.; Panzenboeck, L.; Kasper, C.; Abiead, Y. El; Koellensperger, G.; Lamp, L. M.; Rgen Hartler, J.; Egger, D.; Rampler, E. Decoding Distinct Ganglioside Patterns of Native and Differentiated Mesenchymal Stem Cells by a Novel Glycolipidomics Profiling Strategy. *JACS Au* **2022**. https://doi.org/10.1021/jacsau.2c00230.

(8) Kolter, T. Ganglioside Biochemistry. *ISRN Biochem* **2012**, *2012*, 1–36. https://doi.org/10.5402/2012/506160.
(9) Han, X.; Gross, R. W. Shotgun Lipidomics: Electrospray Ionization Mass Spectrometric Analysis and Quantitation of Cellular Lipidomes Directly from Crude Extracts of Biological Samples. *Mass Spectrom Rev* **2005**, *24* (3), 367–412. https://doi.org/10.1002/MAS.20023.
(10) Köfeler, H. C.; Fauland, A.; Rechberger, G. N.; Trötzmüller, M. Mass Spectrometry Based Lipidomics: An Overview of Technological Platforms. *Metabolites* **2012**, *2* (1), 19. https://doi.org/10.3390/METABO2010019.
(11) Dugo, P.; Cacciola, F.; Kumm, T.; Dugo, G.; Mondello, L. Comprehensive Multidimensional Liquid Chromatography: Theory and Applications. *J Chromatogr A* **2008**, *1184* (1–2), 353–368. https://doi.org/10.1016/J.CHROMA.2007.06.074.
(12) Lísa, M.; Holčapek, M. Triacylglycerols Profiling in Plant Oils Important in Food Industry, Dietetics and Cosmetics Using High-Performance Liquid Chromatography–Atmospheric Pressure Chemical Ionization Mass Spectrometry. *J Chromatogr A* **2008**, *1198–1199* (1–2), 115–130. https://doi.org/10.1016/J.CHROMA.2008.05.037.
(13) Ovčačíková, M.; Lísa, M.; Cífková, E.; Holčapek, M. Retention Behavior of Lipids in Reversed-Phase Ultrahigh-Performance Liquid Chromatography-Electrospray Ionization Mass Spectrometry. *J Chromatogr A* **2016**, *1450*, 76–85. https://doi.org/10.1016/j.chroma.2016.04.082.
(14) Köfeler, H. C.; Eichmann, T. O.; Ahrends, R.; Bowden, J. A.; Danne-Rasche, N.; Dennis, E. A.; Fedorova, M.; Griffiths, W. J.; Han, X.; Hartler, J.; Holčapek, M.; Jirásko, R.; Koelmel, J. P.; Ejsing, C. S.; Liebisch, G.; Ni, Z.; O'Donnell, V. B.; Quehenberger, O.; Schwudke, D.; Shevchenko, A.; Wakelam, M. J. O.; Wenk, M. R.; Wolrab, D.; Ekroos, K. Quality Control Requirements for the Correct Annotation of Lipidomics Data. *Nature Communications 2021 12:1* **2021**, *12* (1), 1–4. https://doi.org/10.1038/S41467-021-24984-Y.
(15) Lakshmi, A.; Gobburi, P.; Kipruto, E. W.; Inman, D. M.; Anderson, D. J. A New LC-MS/MS Technique for Separation of Gangliosides Using a Phenyl-Hexyl Column: Systematic Separation According to Sialic Acid Class and Ceramide Subclass. **2021**. https://doi.org/10.1080/10826076.2020.1856136.
(16) Wormwood Moser, K. L.; Van Aken, G.; DeBord, D.; Hatcher, N. G.; Maxon, L.; Sherman, M.; Yao, L.; Ekroos, K. High-Defined Quantitative Snapshots of the Ganglioside Lipidome Using High Resolution Ion Mobility SLIM Assisted Shotgun Lipidomics. *Anal Chim Acta* **2021**, *1146*, 77–87. https://doi.org/10.1016/J.ACA.2020.12.022.
(17) Sarbu, M.; Robu, A. C.; Ghiulai, R. M.; Vukelić, Ž.; Clemmer, D. E.; Zamfir, A. D. Electrospray Ionization Ion Mobility Mass Spectrometry of Human Brain Gangliosides. *Anal Chem* **2016**, *88* (10), 5166–5178. https://doi.org/10.1021/ACS.ANALCHEM.6B00155.
(18) Zamfir, A.; Vukelić, Ž.; Bindila, L.; Peter-Katalinić, J.; Almeida, R.; Sterling, A.; Allen, M. Fully-Automated Chip-Based Nanoelectrospray Tandem Mass Spectrometry of Gangliosides from Human Cerebellum. *J Am Soc Mass Spectrom* **2004**, *15* (11), 1649–1657. https://doi.org/10.1016/J.JASMS.2004.08.002.
(19) Fujiwara, Y.; Hama, K.; Yokoyama, K. Mass Spectrometry in Combination with a Chiral Column and Multichannel-MRM Allows Comprehensive Analysis of Glycosphingolipid Molecular Species from Mouse Brain. *Carbohydr Res* **2020**, *490*, 107959. https://doi.org/10.1016/J.CARRES.2020.107959.
(20) Hájek, R.; Jirásko, R.; Lísa, M.; Cífková, E.; Holčapek, M. Hydrophilic Interaction Liquid Chromatography-Mass Spectrometry Characterization of Gangliosides in Biological Samples - SupInfo. *Anal Chem* **2017**, *89* (22), 12425–12432. https://doi.org/10.1021/acs.analchem.7b03523.
(21) Kliman, M.; May, J. C.; McLean, J. A. Lipid Analysis and Lipidomics by Structurally Selective Ion Mobility-Mass Spectrometry. *Biochimica et Biophysica Acta (BBA) - Molecular and Cell Biology of Lipids* **2011**, *1811* (11), 935–945. https://doi.org/10.1016/J.BBALIP.2011.05.016.
(22) Dodds, J. N.; Baker, E. S. Ion Mobility Spectrometry: Fundamental Concepts, Instrumentation, Applications, and the Road Ahead. *J Am Soc Mass Spectrom* **2019**, *30* (11), 2185–2195. https://doi.org/10.1007/S13361-019-02288-2/FIGURES/4.
(23) Sarbu, M.; Clemmer, D. E.; Zamfir, A. D. Ion Mobility Mass Spectrometry of Human Melanoma Gangliosides. *Biochimie* **2020**, *177*, 226–237. https://doi.org/10.1016/J.BIOCHI.2020.08.011.
(24) Sarbu, M.; Vukelić, Ž.; Clemmer, D. E.; Zamfir, A. D. Ion Mobility Mass Spectrometry Provides Novel Insights into the Expression and Structure of Gangliosides in the Normal Adult Human Hippocampus. *Analyst* **2018**, *143* (21), 5234–5246. https://doi.org/10.1039/C8AN01118D.
(25) Djambazova, K. V.; Dufresne, M.; Migas, L. G.; Kruse, A. R. S.; Van de Plas, R.; Caprioli, R. M.; Spraggins, J. M. MALDI TIMS IMS of Disialoganglioside Isomers─GD1a and GD1b in Murine Brain Tissue. *Anal Chem* **2023**, *95* (2), 1176–1183. https://doi.org/10.1021/ACS.ANALCHEM.2C03939/ASSET/IMAGES/LARGE/AC2C03939_0006.JPEG.
(26) Fabris, M. ; Vukeli´c, V.; Clemmer, Ž. ; Zamfir, D. E. ; Sarbu, M.; Fabris, D.; Vukeli´c, Ž. V.; Clemmer, D. E.; Zamfir, A. D. Ion Mobility Mass Spectrometry Reveals Rare Sialylated Glycosphingolipid Structures in Human Cerebrospinal Fluid. *Molecules 2022, Vol. 27, Page 743* **2022**, *27* (3), 743. https://doi.org/10.3390/MOLECULES27030743.
(27) Sarbu, M.; Ica, R.; Sharon, E.; Clemmer, D. E.; Zamfir, A. D. Glycomics by Ion Mobility Tandem Mass Spectrometry of Chondroitin Sulfate Disaccharide Domain in Biglycan. *Journal of Mass Spectrometry* **2023**, *58* (3), e4908. https://doi.org/10.1002/JMS.4908.
(28) Sarbu, M.; Raab, S.; Henderson, L.; Fabris, D.; Vukelić, Ž.; Clemmer, D. E.; Zamfir, A. D. Cerebrospinal Fluid: Profiling and Fragmentation of Gangliosides by Ion Mobility Mass Spectrometry. *Biochimie* **2020**, *170*, 36–48. https://doi.org/10.1016/J.BIOCHI.2019.12.008.
(29) Sarbu, M.; Vukelić, Ž.; Clemmer, D. E.; Zamfir, A. D. Electrospray Ionization Ion Mobility Mass Spectrometry Provides Novel Insights into the Pattern and Activity of Fetal Hippocampus Gangliosides. *Biochimie* **2017**, *139*, 81–94. https://doi.org/10.1016/J.BIOCHI.2017.05.016.
(30) Sarbu, M.; Ica, R.; Zamfir, A. D. Developments and Applications of Separation and Microfluidics Methods Coupled to Electrospray Mass Spectrometry in Glycomics of Nervous System Gangliosides. *Electrophoresis* **2021**, *42* (4), 429–449. https://doi.org/10.1002/ELPS.202000236.
(31) Jackson, S. N.; Colsch, B.; Egan, T.; Lewis, E. K.; Schultz, J. A.; Woods, A. S. Gangliosides' Analysis by MALDI-Ion Mobility MS. *Analyst* **2011**, *136* (3), 463. https://doi.org/10.1039/C0AN00732C.
(32) Rajanayake, K. K.; Markus, K.; Isailovic, D. Determination of the Origin of Doubly-Cationized Monosialylated Fragments in MS/MS Spectra of Singly-Cationized LSTb and GM1 Using Ion Mobility Spectrometry-Mass

Spectrometry. *Int J Mass Spectrom* **2017**, *422*, 1–12. https://doi.org/10.1016/J.IJMS.2017.07.007.

(33) May, J. C.; Leaptrot, K. L.; Rose, B. S.; Moser, K. L. W.; Deng, L.; Maxon, L.; Debord, D.; McLean, J. A. Resolving Power and Collision Cross Section Measurement Accuracy of a Prototype High-Resolution Ion Mobility Platform Incorporating Structures for Lossless Ion Manipulation. *J Am Soc Mass Spectrom* **2021**, *32* (4), 1126–1137. https://doi.org/10.1021/JASMS.1C00056/ASSET/IMAGES/LARGE/JS1C00056_0005.JPEG.

(34) Škrášková, K.; Claude, E.; Jones, E. A.; Towers, M.; Ellis, S. R.; Heeren, R. M. A. Enhanced Capabilities for Imaging Gangliosides in Murine Brain with Matrix-Assisted Laser Desorption/Ionization and Desorption Electrospray Ionization Mass Spectrometry Coupled to Ion Mobility Separation. *Methods* **2016**, *104*, 69–78. https://doi.org/10.1016/J.YMETH.2016.02.014.

(35) Feider, C. L.; Elizondo, N.; Eberlin, L. S. Ambient Ionization and FAIMS Mass Spectrometry for Enhanced Imaging of Multiply Charged Molecular Ions in Biological Tissues. *Anal Chem* **2016**, *88* (23), 11533–11541. https://doi.org/10.1021/ACS.ANALCHEM.6B02798/ASSET/IMAGES/LARGE/AC-2016-02798E_0006.JPEG.

(36) Xia, Y. Q.; Wu, S. T.; Jemal, M. LC-FAIMS-MS/MS for Quantification of a Peptide in Plasma and Evaluation of FAIMS Global Selectivity from Plasma Components. *Anal Chem* **2008**, *80* (18), 7137–7143. https://doi.org/10.1021/AC8010846/ASSET/IMAGES/LARGE/AC-2008-010846_0002.JPEG.

(37) Swearingen, K. E.; Moritz, R. L. High Field Asymmetric Waveform Ion Mobility Spectrometry (FAIMS) for Mass Spectrometry-Based Proteomics. *Expert Rev Proteomics* **2012**, *9* (5), 505. https://doi.org/10.1586/EPR.12.50.

(38) Schnirch, L.; Nadler-Holly, M.; Siao, S. W.; Frese, C. K.; Viner, R.; Liu, F. Expanding the Depth and Sensitivity of Cross-Link Identification by Differential Ion Mobility Using High-Field Asymmetric Waveform Ion Mobility Spectrometry. *Anal Chem* **2020**, *92* (15), 10495–10503. https://doi.org/10.1021/ACS.ANALCHEM.0C01273/ASSET/IMAGES/LARGE/AC0C01273_0006.JPEG.

(39) Kralj, T.; Nuske, M.; Hofferek, V.; Sani, M. A.; Lee, T. H.; Separovic, F.; Aguilar, M. I.; Reid, G. E. Multi-Omic Analysis to Characterize Metabolic Adaptation of the E. Coli Lipidome in Response to Environmental Stress. *Metabolites* **2022**, *12* (2). https://doi.org/10.3390/metabo12020171.

(40) Johnson, K. R.; Greguš, M.; Ivanov, A. R. Coupling High-Field Asymmetric Ion Mobility Spectrometry with Capillary Electrophoresis-Electrospray Ionization-Tandem Mass Spectrometry Improves Protein Identifications in Bottom-Up Proteomic Analysis of Low Nanogram Samples. *J Proteome Res* **2022**, *21* (10), 2453. https://doi.org/10.1021/ACS.JPROTEOME.2C00337.

(41) Venne, K.; Bonneil, E.; Eng, K.; Thibault, P. Improvement in Peptide Detection for Proteomics Analyses Using NanoLC-MS and High-Field Asymmetry Waveform Ion Mobility Mass Spectrometry. *Anal Chem* **2005**, *77* (7), 2176–2186. https://doi.org/10.1021/AC048410J/ASSET/IMAGES/LARGE/AC048410JF00009.JPEG.

(42) Sweet, S.; Chain, D.; Yu, W.; Martin, P.; Rebelatto, M.; Chambers, A.; Cecchi, F.; Kim, Y. J. The Addition of FAIMS Increases Targeted Proteomics Sensitivity from FFPE Tumor Biopsies. *Scientific Reports 2022 12:1* **2022**, *12* (1), 1–10. https://doi.org/10.1038/S41598-022-16358-1.

(43) Fang, W.; Du, Z.; Kong, L.; Fu, B.; Wang, G.; Zhang, Y.; Qin, W. A Rapid and Sensitive Single-Cell Proteomic Method Based on Fast Liquid-Chromatography Separation, Retention Time Prediction and MS1-Only Acquisition. *Anal Chim Acta* **2023**, *1251*, 341038. https://doi.org/10.1016/J.ACA.2023.341038.

(44) Berthias, F.; Poad, B. L. J.; Thurman, H. A.; Bowman, A. P.; Blanksby, S. J.; Shvartsburg, A. A. Disentangling Lipid Isomers by High-Resolution Differential Ion Mobility Spectrometry/Ozone-Induced Dissociation of Metalated Species. *J Am Soc Mass Spectrom* **2021**, *32* (12), 2827–2836. https://doi.org/10.1021/JASMS.1C00251/ASSET/IMAGES/LARGE/JS1C00251_0008.JPEG.

(45) Fernández Requena, B.; Nadeem, S.; Reddy, V. P.; Naidoo, V.; Glasgow, J. N.; Steyn, A. J. C.; Barbas, C.; Gonzalez-Riano, C. LiLA: Lipid Lung-Based ATLAS Built through a Comprehensive Workflow Designed for an Accurate Lipid Annotation. *Communications Biology 2024 7:1* **2024**, *7* (1), 1–16. https://doi.org/10.1038/s42003-023-05680-7.

(46) O'Brien, J. P.; Brodbelt, J. S. Structural Characterization of Gangliosides and Glycolipids via Ultraviolet Photodissociation Mass Spectrometry. *Anal Chem* **2013**, *85* (21), 10399–10407. https://doi.org/10.1021/AC402379Y.

(47) Williams, P. E.; Klein, D. R.; Greer, S. M.; Brodbelt, J. S. Pinpointing Double Bond and Sn-Positions in Glycerophospholipids via Hybrid 193 Nm Ultraviolet Photodissociation (UVPD) Mass Spectrometry. *J Am Chem Soc* **2017**, *139* (44), 15681–15690. https://doi.org/10.1021/JACS.7B06416/SUPPL_FILE/JA7B06416_SI_001.PDF.

(48) Macias, L. A.; Garza, K. Y.; Feider, C. L.; Eberlin, L. S.; Brodbelt, J. S. Relative Quantitation of Unsaturated Phosphatidylcholines Using 193 Nm Ultraviolet Photodissociation Parallel Reaction Monitoring Mass Spectrometry. *J Am Chem Soc* **2021**, *143* (36), 14622–14634. https://doi.org/10.1021/JACS.1C05295/ASSET/IMAGES/LARGE/JA1C05295_0006.JPEG.

(49) Klein, D. R.; Brodbelt, J. S. Structural Characterization of Phosphatidylcholines Using 193 Nm Ultraviolet Photodissociation Mass Spectrometry. *Anal Chem* **2017**, *89* (3), 1516–1522. https://doi.org/10.1021/acs.analchem.6b03353.

(50) Ryan, E.; Nguyen, C. Q. N.; Shiea, C.; Reid, G. E. Detailed Structural Characterization of Sphingolipids via 193 Nm Ultraviolet Photodissociation and Ultra High Resolution Tandem Mass Spectrometry. *J Am Soc Mass Spectrom* **2017**, *28* (7), 1406–1419. https://doi.org/10.1007/S13361-017-1668-1/SUPPL_FILE/JS8B05595_SI_001.PDF.

(51) Blevins, M. S.; Klein, D. R.; Brodbelt, J. S. Localization of Cyclopropane Modifications in Bacterial Lipids via 213 Nm Ultraviolet Photodissociation Mass Spectrometry. *Anal Chem* **2019**, *91* (10), 6820–6828. https://doi.org/10.1021/ACS.ANALCHEM.9B01038/ASSET/IMAGES/LARGE/AC-2019-01038C_0006.JPEG.

(52) Macias, L. A.; Feider, C. L.; Eberlin, L. S.; Brodbelt, J. S. Hybrid 193 Nm Ultraviolet Photodissociation Mass Spectrometry Localizes Cardiolipin Unsaturations. *Anal Chem* **2019**, *91* (19), 12509–12516. https://doi.org/10.1021/ACS.ANALCHEM.9B03278/SUPPL_FILE/AC9B03278_SI_001.PDF.

(53) Fang, M.; Rustam, Y.; Palmieri, M.; Sieber, O. M.; Reid, G. E. Evaluation of Ultraviolet Photodissociation Tandem Mass Spectrometry for the Structural Assignment of Unsaturated Fatty Acid Double Bond Positional Isomers.

Anal Bioanal Chem **2020**, *412* (10), 2339–2351. https://doi.org/10.1007/S00216-020-02446-6/FIGURES/7.

(54) Buenger, E. W.; Reid, G. E. Shedding Light on Isomeric FAHFA Lipid Structures Using 213 Nm Ultraviolet Photodissociation Mass Spectrometry. *European Journal of Mass Spectrometry* **2020**, *26* (5), 311–323. https://doi.org/10.1177/1469066720960341.

(55) West, H.; Reid, G. E. Hybrid 213 Nm Photodissociation of Cationized Sterol Lipid Ions Yield [M]+. Radical Products for Improved Structural Characterization Using Multistage Tandem Mass Spectrometry. *Anal Chim Acta* **2021**, *1141*, 100–109. https://doi.org/10.1016/J.ACA.2020.10.013.

(56) Blevins, M. S.; Shields, S. W. J.; Cui, W.; Fallatah, W.; Moser, A. B.; Braverman, N. E.; Brodbelt, J. S. Structural Characterization and Quantitation of Ether-Linked Glycerophospholipids in Peroxisome Biogenesis Disorder Tissue by Ultraviolet Photodissociation Mass Spectrometry. *Anal Chem* **2022**, *94* (37), 12621–12629. https://doi.org/10.1021/ACS.ANALCHEM.2C01274/SUPPL_FILE/AC2C01274_SI_001.PDF.

(57) Klein, D. R.; Blevins, M. S.; MacIas, L. A.; Douglass, M. V.; Trent, M. S.; Brodbelt, J. S. Localization of Double Bonds in Bacterial Glycerophospholipids Using 193 Nm Ultraviolet Photodissociation in the Negative Mode. *Anal Chem* **2020**, *92* (8), 5986–5993. https://doi.org/10.1021/ACS.ANALCHEM.0C00221/SUPPL_FILE/AC0C00221_SI_001.PDF.

(58) Ni, Z.; Wölk, M.; Jukes, G.; Mendivelso Espinosa, K.; Ahrends, R.; Aimo, L.; Alvarez-Jarreta, J.; Andrews, S.; Andrews, R.; Bridge, A.; Clair, G. C.; Conroy, M. J.; Fahy, E.; Gaud, C.; Goracci, L.; Hartler, J.; Hoffmann, N.; Kopczyinki, D.; Korf, A.; Lopez-Clavijo, A. F.; Malik, A.; Ackerman, J. M.; Molenaar, M. R.; O'Donovan, C.; Pluskal, T.; Shevchenko, A.; Slenter, D.; Siuzdak, G.; Kutmon, M.; Tsugawa, H.; Willighagen, E. L.; Xia, J.; O'Donnell, V. B.; Fedorova, M. Guiding the Choice of Informatics Software and Tools for Lipidomics Research Applications. *Nature Methods 2022 20:2* **2022**, *20* (2), 193–204. https://doi.org/10.1038/S41592-022-01710-0.

(59) Herzog, R.; Schuhmann, K.; Schwudke, D.; Sampaio, J. L.; Bornstein, S. R.; Schroeder, M.; Shevchenko, A. LipidXplorer: A Software for Consensual Cross-Platform Lipidomics. *PLoS One* **2012**, *7* (1), e29851. https://doi.org/10.1371/JOURNAL.PONE.0029851.

(60) Hartler, J.; Trötzmüller, M.; Chitraju, C.; Spener, F.; Köfeler, H. C.; Thallinger, G. G. Lipid Data Analyzer: Unattended Identification and Quantitation of Lipids in LC-MS Data. *Bioinformatics* **2011**, *27* (4), 572–577. https://doi.org/10.1093/BIOINFORMATICS/BTQ699.

(61) Hartler, J.; Triebl, A.; Ziegl, A.; Trötzmüller, M.; Rechberger, G. N.; Zeleznik, O. A.; Zierler, K. A.; Torta, F.; Cazenave-Gassiot, A.; Wenk, M. R.; Fauland, A.; Wheelock, C. E.; Armando, A. M.; Quehenberger, O.; Zhang, Q.; Wakelam, M. J. O.; Haemmerle, G.; Spener, F.; Köfeler, H. C.; Thallinger, G. G. Deciphering Lipid Structures Based on Platform-Independent Decision Rules. *Nature Methods 2017 14:12* **2017**, *14* (12), 1171–1174. https://doi.org/10.1038/NMETH.4470.

(62) Hartler, J.; Armando, A. M.; Trötzmüller, M.; Dennis, E. A.; Köfeler, H. C.; Quehenberger, O. Automated Annotation of Sphingolipids Including Accurate Identification of Hydroxylation Sites Using MS n Data. *Anal Chem* **2020**, *92* (20), 14054–14062. https://doi.org/10.1021/ACS.ANALCHEM.0C03016.

(63) MacLean, B.; Tomazela, D. M.; Shulman, N.; Chambers, M.; Finney, G. L.; Frewen, B.; Kern, R.; Tabb, D. L.; Liebler, D. C.; MacCoss, M. J. Skyline: An Open Source Document Editor for Creating and Analyzing Targeted Proteomics Experiments. *Bioinformatics* **2010**, *26* (7), 966–968. https://doi.org/10.1093/BIOINFORMATICS/BTQ054.

(64) Stejskal, K.; De Beeck, J. O.; Durnberger, G.; Jacobs, P.; Mechtler, K. Ultrasensitive NanoLC-MS of Subnanogram Protein Samples Using Second Generation Micropillar Array LC Technology with Orbitrap Exploris 480 and FAIMS PRO. *Anal Chem* **2021**, *93*, 8710. https://doi.org/10.1021/ACS.ANALCHEM.1C00990/ASSET/IMAGES/LARGE/AC1C00990_0003.JPEG.

(65) Ang, C. S.; Sacharz, J.; Leeming, M. G.; Nie, S.; Varshney, S.; Scott, N. E.; Williamson, N. A. Getting More out of FLAG-Tag Co-Immunoprecipitation Mass Spectrometry Experiments Using FAIMS. *J Proteomics* **2022**, *254*, 104473. https://doi.org/10.1016/J.JPROT.2021.104473.

(66) Hoffmann, N.; Rein, J.; Sachsenberg, T.; Hartler, J.; Haug, K.; Mayer, G.; Alka, O.; Dayalan, S.; Pearce, J. T. M.; Rocca-Serra, P.; Qi, D.; Eisenacher, M.; Perez-Riverol, Y.; Vizcaíno, J. A.; Salek, R. M.; Neumann, S.; Jones, A. R. MzTab-M: A Data Standard for Sharing Quantitative Results in Mass Spectrometry Metabolomics. *Anal Chem* **2019**, *91* (5), 3302–3310. https://doi.org/10.1021/ACS.ANALCHEM.8B04310/ASSET/IMAGES/LARGE/AC-2018-04310D_0003.JPEG.

(67) Schwudke, D.; Liebisch, G.; Herzog, R.; Schmitz, G.; Shevchenko, A. Shotgun Lipidomics by Tandem Mass Spectrometry under Data-Dependent Acquisition Control. *Methods Enzymol* **2007**, *433*, 175–191. https://doi.org/10.1016/S0076-6879(07)33010-3.

(68) Bowden, J. A.; Heckert, A.; Ulmer, C. Z.; Jones, C. M.; Koelmel, J. P.; Abdullah, L.; Ahonen, L.; Alnouti, Y.; Armando, A. M.; Asara, J. M.; Bamba, T.; Barr, J. R.; Bergquist, J.; Borchers, C. H.; Brandsma, J.; Breitkopf, S. B.; Cajka, T.; Cazenave-Gassiot, A.; Checa, A.; Cinel, M. A.; Colas, R. A.; Cremers, S.; Dennis, E. A.; Evans, J. E.; Fauland, A.; Fiehn, O.; Gardner, M. S.; Garrett, T. J.; Gotlinger, K. H.; Han, J.; Huang, Y.; Neo, A. H.; Hyötyläinen, T.; Izumi, Y.; Jiang, H.; Jiang, H.; Jiang, J.; Kachman, M.; Kiyonami, R.; Klavins, K.; Klose, C.; Köfeler, H. C.; Kolmert, J.; Koal, T.; Koster, G.; Kuklenyik, Z.; Kurland, I. J.; Leadley, M.; Lin, K.; Maddipati, K. R.; McDougall, D.; Meikle, P. J.; Mellett, N. A.; Monnin, C.; Moseley, M. A.; Nandakumar, R.; Oresic, M.; Patterson, R.; Peake, D.; Pierce, J. S.; Post, M.; Postle, A. D.; Pugh, R.; Qiu, Y.; Quehenberger, O.; Ramrup, P.; Rees, J.; Rembiesa, B.; Reynaud, D.; Roth, M. R.; Sales, S.; Schuhmann, K.; Schwartzman, M. L.; Serhan, C. N.; Shevchenko, A.; Somerville, S. E.; St John-Williams, L.; Surma, M. A.; Takeda, H.; Thakare, R.; Thompson, J. W.; Torta, F.; Triebl, A.; Trötzmüller, M.; Ubhayasekera, S. J. K.; Vuckovic, D.; Weir, J. M.; Welti, R.; Wenk, M. R.; Wheelock, C. E.; Yao, L.; Yuan, M.; Zhao, X. H.; Zhou, S. Harmonizing Lipidomics: NIST Interlaboratory Comparison Exercise for Lipidomics Using SRM 1950–Metabolites in Frozen Human Plasma [S]. *J Lipid Res* **2017**, *58* (12), 2275–2288. https://doi.org/10.1194/JLR.M079012.

(69) Dautel, S. E.; Kyle, J. E.; Clair, G.; Sontag, R. L.; Weitz, K. K.; Shukla, A. K.; Nguyen, S. N.; Kim, Y. M.; Zink, E. M.; Luders, T.; Frevert, C. W.; Gharib, S. A.; Laskin, J.; Carson, J. P.; Metz, T. O.; Corley, R. A.; Ansong, C. Lipidomics Reveals Dramatic Lipid Compositional Changes

in the Maturing Postnatal Lung. *Scientific Reports 2017 7:1* **2017**, *7* (1), 1–12. https://doi.org/10.1038/srep40555.

(70) Ooi, G. J.; Meikle, P. J.; Huynh, K.; Earnest, A.; Roberts, S. K.; Kemp, W.; Parker, B. L.; Brown, W.; Burton, P.; Watt, M. J. Hepatic Lipidomic Remodeling in Severe Obesity Manifests with Steatosis and Does Not Evolve with Non-Alcoholic Steatohepatitis. *J Hepatol* **2021**, *75* (3), 524–535. https://doi.org/10.1016/j.jhep.2021.04.013.

(71) Salihovic, S.; Lamichane, S.; Hyötyläinen, T.; Orešič, M. Recent Advances towards Mass Spectrometry-Based Clinical Lipidomics. *Curr Opin Chem Biol* **2023**, *76*, 102370. https://doi.org/10.1016/J.CBPA.2023.102370.

(72) Liebisch, G.; Fahy, E.; Aoki, J.; Dennis, E. A.; Durand, T.; Ejsing, C. S.; Fedorova, M.; Feussner, I.; Griffiths, W. J.; Köfeler, H.; Merrill, A. H.; Murphy, R. C.; O'Donnell, V. B.; Oskolkova, O.; Subramaniam, S.; Wakelam, M. J. O.; Spener, F. Update on LIPID MAPS Classification, Nomenclature, and Shorthand Notation for MS-Derived Lipid Structures. *J Lipid Res* **2020**, *61* (12), 1539–1555. https://doi.org/10.1194/jlr.S120001025.

(73) Varki, A.; Cummings, R. D.; Aebi, M.; Packer, N. H.; Seeberger, P. H.; Esko, J. D.; Stanley, P.; Hart, G.; Darvill, A.; Kinoshita, T.; Prestegard, J. J.; Schnaar, R. L.; Freeze, H. H.; Marth, J. D.; Bertozzi, C. R.; Etzler, M. E.; Frank, M.; Vliegenthart, J. F. G.; Lütteke, T.; Perez, S.; Bolton, E.; Rudd, P.; Paulson, J.; Kanehisa, M.; Toukach, P.; Aoki-Kinoshita, K. F.; Dell, A.; Narimatsu, H.; York, W.; Taniguchi, N.; Kornfeld, S. Symbol Nomenclature for Graphical Representations of Glycans. *Glycobiology* **2015**, *25* (12), 1323–1324. https://doi.org/10.1093/GLYCOB/CWV091.

(74) Neelamegham, S.; Aoki-Kinoshita, K.; Bolton, E.; Frank, M.; Lisacek, F.; Lütteke, T.; O'Boyle, N.; Packer, N. H.; Stanley, P.; Toukach, P.; Varki, A.; Woods, R. J. Updates to the Symbol Nomenclature for Glycans Guidelines. *Glycobiology* **2019**, *29* (9), 620. https://doi.org/10.1093/GLYCOB/CWZ045.

(75) Guo, Z. Ganglioside GM1 and the Central Nervous System. *International Journal of Molecular Sciences 2023, Vol. 24, Page 9558* **2023**, *24* (11), 9558. https://doi.org/10.3390/IJMS24119558.

(76) Waki, H.; Murata, A.; Kon, K.; Maruyama, K.; Kimura, S.; Ogura, H.; Ando, S. Isolation and Characterization of a Trisialyllactosylceramide, GT3, Containing an O-Acetylated Sialic Acid in Cod Fish Brain. *J Biochem* **1993**, *113* (4), 502–507. https://doi.org/10.1093/OXFORDJOURNALS.JBCHEM.A124073.

(77) Freischütz, B.; Saito, M.; Rahmann, H.; Yu, R. K. Activities of Five Different Sialyltransferases in Fish and Rat Brains. *J Neurochem* **1994**, *62* (5), 1965–1973. https://doi.org/10.1046/J.1471-4159.1994.62051965.X.